Nuclear Engineering and Technology 54 (2022) 3250–3259

Contents lists available at ScienceDirect

Nuclear Engineering and Technology

journal homepage: www.elsevier.com/locate/net

Original Article

A novel approach for rice straw agricultural waste utilization: Synthesis of solid aluminosilicate matrices for cesium immobilization

A.E. Panasenko [a], O.O. Shichalin [b, *], S.B. Yarusova [a, c], A.I. Ivanets [d], A.A. Belov [b], A.N. Dran'kov [a, b], S.A. Azon [b], A.N. Fedorets [b], I. Yu Buravlev [a, b], V. Yu Mayorov [a, b], D. Kh Shlyk [a], A.A. Buravleva [b], E.B. Merkulov [a], N.V. Zarubina [e], E.K. Papynov [b]

[a] Institute of Chemistry, Far Eastern Branch of Russian Academy of Sciences, 159, Prosp. 100-letiya Vladivostoka, Vladivostok, 690022, Russia
[b] Far Eastern Federal University, 10 Ajax Bay, Russky Island, 690922, Vladivostok, Russia
[c] Vladivostok State University of Economics and Service, Gogolya st., 41, Vladivostok, 690014, Russia
[d] Institute of General and Inorganic Chemistry of National Academy of Sciences of Belarus, Surganova st. 9/1, Minsk, 220072, Belarus
[e] Far East Geological Institute, Far Eastern Branch of Russian Academy of Sciences, 159, Prosp. 100-letiya Vladivostoka, Vladivostok, 690022, Russia

ARTICLE INFO

Article history:
Received 1 January 2022
Received in revised form
22 March 2022
Accepted 5 April 2022
Available online 9 April 2022

Keywords:
Rice straw
Agriculture waste utilization
Glass–ceramic matrices
Radionuclide immobilization
Potassium aluminosilicate

ABSTRACT

A new approach to the use of rice straw as a difficult-to-recycle agricultural waste was proposed. Potassium aluminosilicate was obtained by spark plasma sintering as an effective material for subsequent immobilization of ^{137}Cs into a solid-state matrix. The sorption properties of potassium aluminosilicate to ^{137}Cs from aqueous solutions were studied. The effect of the synthesis temperature on the phase composition, microstructure, and rate of cesium leaching from samples obtained at 800–1000 °C and a pressure of 25 MPa was investigated. It was shown that the positive dynamics of compaction was characteristic of glass ceramics throughout the sintering. Glass ceramics RS-$(K,Cs)AlSi_3O_8$ obtained by the SPS method at 1000 °C for 5 min was characterized by a high density of ~2.62 g/cm^3, Vickers hardness ~ 2.1 GPa, compressive strength ~231.3 MPa and the rate of cesium ions leaching of ~1.37 × 10^{-7} g cm^{-2}·day^{-1}. The proposed approach makes it possible to safe dispose of rice straw and reduce emissions into the atmosphere of microdisperse amorphous silica, which is formed during its combustion and causes respiratory diseases, including cancer. In addition, the obtained is perspective to solve the problem of recycling long-lived ^{137}Cs radionuclides formed during the operation of nuclear power plants into solid-state matrices.

1. Introduction

The acute problem of global climate change is associated with the carbon footprint of human activity, including carbon dioxide emissions during the operation of thermal power plants (TPPs) on gas, coal and fuel oil [1,2]. One way to reduce such emissions is to use sustainable permanent energy sources, such as nuclear power. Nuclear power plants currently provide about 13% of the world's electricity and have become a reliable source of electricity for the base load [3]. However, accidents occur at nuclear power plants, one of which, at the Fukushima Daiichi station, was caused by the Tohoku earthquake and tsunami in eastern Japan on March 11, 2011 [4]. The accident was assigned a maximum level of 7 on the International Nuclear Event Scale (INES).

In order for nuclear power to meet the requirements of reliability, safety and economy, it is necessary to solve a number of problems related to materials. One of the problems associated with nuclear power plants is the resulting highly active nuclear waste. The disposal scheme implies their burial in underground storage facilities, but in order to guarantee safety, radioactive waste must have high resistance to the external environment. To do this, radioactive elements must be immobilized in the form of compounds of such a composition that will be resistant to the effects of destructive environmental factors during their prolonged exposure, such as high temperatures, thermal stresses, radiation exposure, corrosive effects of water and chemical solutions.

Nature-like materials similar to a stable mineral are preferred for radionuclides immobilization. Pollucite $CsAlSi_2O_6$ is considered the preferred mineral for ^{137}Cs immobilization [5–8]. However, the

* Corresponding author.
E-mail address: oleg_shich@mail.ru (O.O. Shichalin).

https://doi.org/10.1016/j.net.2022.04.005

synthesis of pollucite requires a fairly high consolidation temperature (>1000 °C) [5,9], at which cesium easily volatilizes. It was shown shows the prospects of using inorganic sorption materials for cesium radionuclides adsorption, such as the non-mica aluminosilicate minerals kaolinite, galloisite, chlorite, montmorillonite, mordenite, as well as MnO_2, TiO_2, Al_2O_3 and FeOOH [10–14].

On the other hand, there is a significant problem of recycling agricultural waste from rice production. Due to the fact that rice is a silicophilic plant and contains up to 29% silicon dioxide [15], the processing of rice husks and straw presents certain difficulties. Currently, straw and rice husks are mostly plowed in the fields or burned [10], but it slowly decomposes in the soil due to the surface wax layer, and when it is burned, microparticles of silicon dioxide enter the air, causing lung diseases, including cancer, in the population in areas where rice is grown [16,17]. The use of rice straw as a source of silicon and raw materials for the synthesis of aluminosilicates makes it possible to solve the environmental problem of recycling this agricultural waste. And if rice husk is relatively studied and used for the synthesis of aluminosilicates [17–19], then there are significantly fewer studies on rice straw [10,20], despite the fact that rice straw produces the purest silica and is better suited for the preparation of silicate materials [15].

Silicate and aluminosilicate materials are of interest due to their sorption properties to heavy metal ions [21–23], radionuclides [6,24–26], organic dyes [27,28] and other pollutants. Such materials are used, among other things, for cleaning solutions in medicine [29], concentrations of scattered and rare earth elements [30], as matrices for catalysts with embedded transition metals [31]. Moreover, both materials based on natural raw materials (zeolite, vermiculite, etc.) and their synthetic analogues can be used for these purposes [32].

Synthetic aluminosilicates have a number of advantages: constant composition, reproducibility of properties, absence of impurities. The use of vegetable silicon-containing raw materials - rice straw, makes it possible to obtain silicon-containing materials with a low content of impurities without additional purification procedures [33]. To obtain aluminosilicates from rice straw, the most convenient method is alkaline leaching of silicon from vegetable raw materials [7,20], and its further interaction with aluminum compounds. It is known that such raw materials as geopolymer composites based on metacaolin and volcanic ash [10,34], bauxite minerals based on $Al(OH)_3$ [35], aluminum foil [36], aluminum cans [37] and aluminum slag [38] are used as a source of aluminum.

The work aimed to obtain $KAlSi_3O_8$ from rice straw by the SPS method as a perspective matrices for cesium immobilization. The novelty of the work was due to: (i) a method for obtaining $KAlSi_3O_8$ aluminosilicate using agricultural waste - rice straw as a renewable raw; (ii) the physico-chemical and adsorption properties of the prepared aluminosilicate to cesium ions were studied; (iii) the high efficiency of reliable immobilization of cesium ions into solid-state matrices was experimentally proved.

2. Experimental

2.1. Synthesis of potassium–Cesium aluminosilicate from rice straw (RS-(K,Cs)$AlSi_3O_8$)

Rice straw of the "Meadow" variety of the Far Eastern selection was washed with water, crushed into pieces 2–5 cm, dried in air. Then the straw was treated with 1 M KOH solution in the ratio S:L = 1:25 g/mL for 1 h at 95 °C. The resulting solution was separated by filtration and, with intensive stirring at 95 °C, a 0.5 M $Al_2(SO_4)_3 \cdot 18H_2O$ solution was slowly added to it in an amount of 2% of the reaction mixture volume. The precipitate was separated by filtration, washed with water and dried in air at 105 °C. The product was a fine powder of beige color, the yield was 18 wt % of the initial straw, the elemental composition corresponds to the formula RS-$KAlSi_3O_8$.

The saturation of the obtained material with cesium was carried out from an aqueous 0.2 M CsCl solution at room temperature with stirring for 1 h. The sorbent saturated with cesium was separated on a filter, washed once with water and dried in air at 105 °C. The scheme of the experiment is shown in Fig. 1.

2.2. Spark plasma sintering of RS-(K,Cs)$AlSi_3O_8$ solid matrices

SPS of potassium-cesium aluminosilicate from rice straw RS-(K,Cs)$AlSi_3O_8$ matrices was conducted on a LABOX-625 (Japan) installment: reactive mixture was put into cylindrical graphite die (outer diameter 30 mm, internal diameter 15.3 mm, height 30 mm), prepressed (20.7 MPa), further the green body was transferred into a vacuum chamber (6 Pa) and sintered. Heating was conducted by the pulse current in the On/Off regime with the periodicity of the pulse/pause of 12/2 (39.6/6.6 ms). Synthesis temperature was 800, 900, 1000 °C, heating rate – 100 °C min holding time at maximal temperature and cooling were 5 and 30 min, respectively; uniaxial pressure load during sintering was maintained constant at 24.5 MPa. The obtained samples were cylindrical with a diameter of 15.3 mm and height 4–6 mm.

2.3. Characterization methods

Cesium, aluminum, potassium concentration in solutions being found on an inductively coupled plasma mass spectrometry on an Agilent 8800 spectrometer (Agilent Techn., USA). Particle size distribution was determined on a particle size analyzer Analysette-22

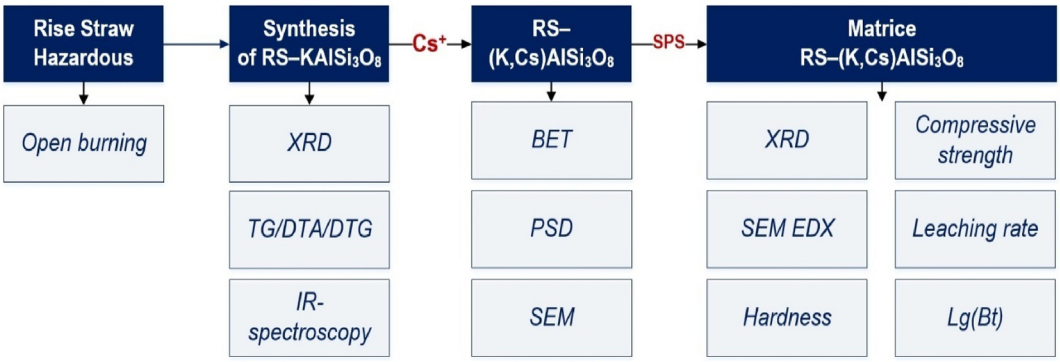

Fig. 1. Scheme of experiment.

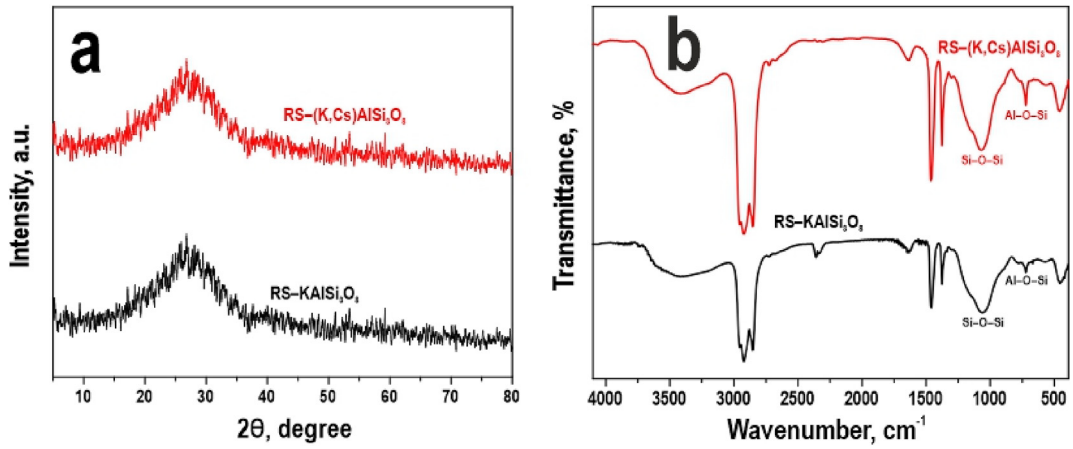

Fig. 2. (a) XRD and (b) FT-IR spectra of RS-$KAlSi_3O_8$ and RS-$(K,Cs)AlSi_3O_8$ aluminosilicates.

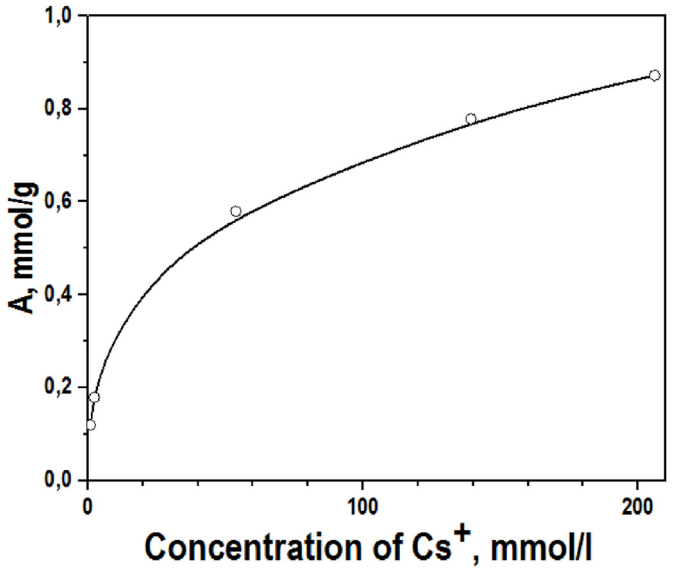

Fig. 3. Sorption isotherm of cesium ions on RS-$KAlSi_3O_8$ aluminosilicate.

NanoTec/MicroTec/XT "Fritsch" (Germany). Scanning electron microscopy (SEM) was done on a CrossBeam 1540 XB "Carl Zeiss" (Germany) equipped with the add-on for energy-dispersive spectral analysis (EDX) "Bruker" (Germany). XRD was carried out on a "D8 Advance Bruker AXS" (Germany) diffractometer. Vickers microhardness (HV) was determined at 0.2 N load on a microhardness tester HMV-G-FA-D "Shimadzu" (Japan). Compressive strength (σcs.) was evaluated on a tensile machine Autograph AG-X plus 100 kN "Shimadzu" (Japan). Experimental density (ED) was measured by hydrostatic weighing on the balance Adventurer™ "OHAUS Corporation" (USA). Relative density (RD) was found as a ratio of the experimental density (ED) measured via hydrostatic weighing to the theoretical density (TD). The thermogravimetric study was carried out on a STA 449C (NETZSCH) device in platinum crucibles with a pierced lid in a dry argon stream (20 mL/min) in the temperature range of 35–1300 °C and a heating rate of 10 °C/min. The weight of the canopies was about 40 mg, weighing was carried out on Sartorius CP2P microweights with an accuracy of 1 μg.

2.4. Evolution of cesium leaching from RS-$(K,Cs)AlSi_3O_8$ matrices

Evolution of cesium leaching from RS-$(K,Cs)AlSi_3O_8$ matrices was estimated based on desalination rate of cesium under long-term contact (30 days) with the distilled water (pH 6.8) at room temperature (25°C) in static condition according to well-known Russian Government Standard (GOST R 52126–2003), closely related to the ANSI/ANS-American National Standards Institute/American Nuclear Society 2019 (ANSI/ANS 16.1) that was updated according to the older procedure recommended by IAEA (ISO 6961:1982).

Long time leach testing of solidified radioactive waste forms" the leaching of solidified samples was carried out in prolonged contact with distilled water. In the process we selected samples of the contact solution in the volume of 5 ml during the given time interval.

Thus, the leaching rate was calculated according to the following formula:

$$R_n^i = \frac{m_{\Pi}^i}{M_0^i \times t_n \times S} \quad (1)$$

where R_n^i - leaching rate, g/(cm^2*days);

m_{Π}^i - mass of the i-th element leached during the n-th test time interval, g;
M_0^i - mass concentration of the i-th element in the matrix, g/g;
S - surface area of the sample, cm^2;
t_n- time of testing of the sample, day.

The volume of the contacted solution was taken equal to 25 ml, according to the recommendation on the ratio of the solution volume to the sample area (3–10 cm). Thus, for the presented samples KAlSi3O8 800, 900, 1000 the ratios were 6.8 cm, 13 cm, 9 cm, respectively. Sampling was performed after 1, 3, 7, 14, 21, and 28 days, respectively.

The calculation of the effective diffusion coefficient (D_e) was carried out by mathematical transformations of the second Fick law according to the methodology described in the work [39]:

$$\frac{\sum m}{M_0} = 2\left(\frac{D_e}{\pi}\right)^{\frac{1}{2}}\left(\frac{S}{V}\right)t^{\frac{1}{2}} + \alpha \quad (2)$$

where m is the mass of cesium (mg) leached over a time interval t, s,

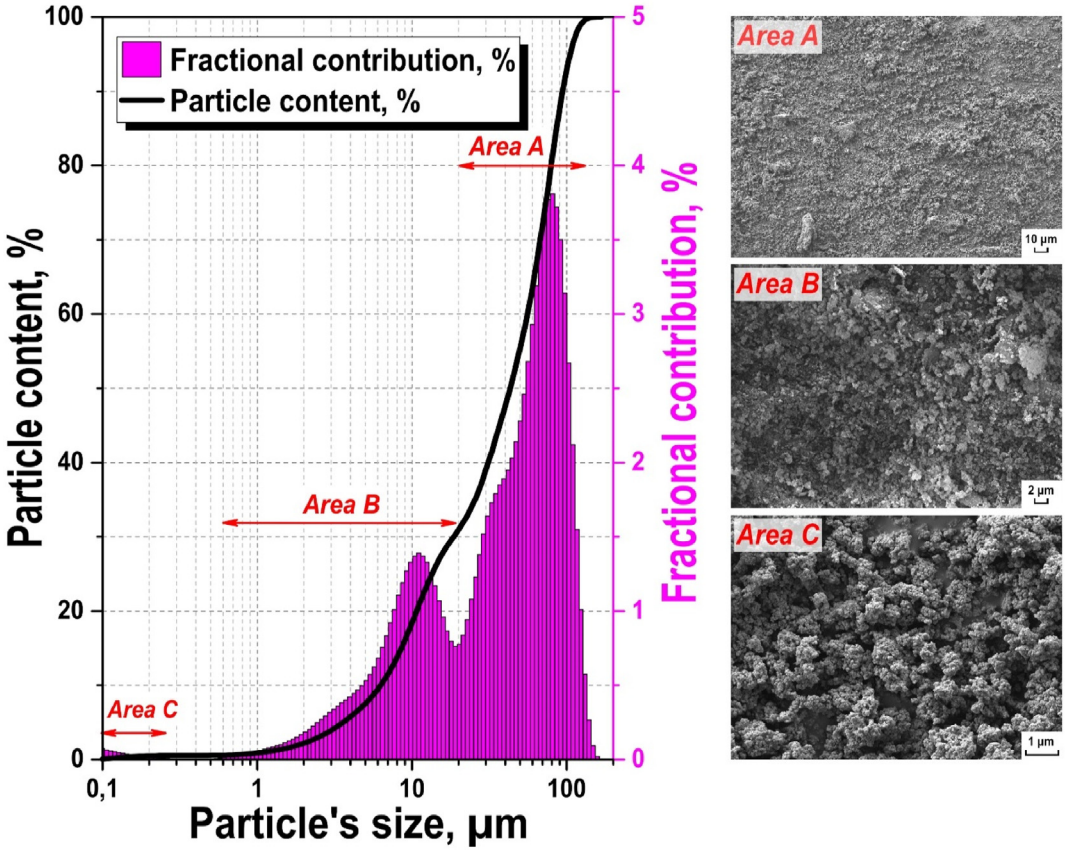

Fig. 4. Particle size distribution (a) and SEM images (b, c and d) of RS-(K,Cs)$AlSi_3O_8$ powder.

M_0 is the initial amount of cesium in the sample, mg, D_e is the effective diffusion coefficient, cm^2/s, S is the surface area of the sample, cm^2, V is the volume of the sample, cm^3, α is a parameter that takes into account the initial cesium leaching (not related to diffusion displacement, cesium is leached at the initial contact of the aqueous solution with the sample surface).

To calculate this equation, this equation was reduced to a linear form by introducing the coefficient K, which is the tangent of the slope angle of the direct dependence of the cesium fraction leached from the sample on the square root of the contact time of the material with the leaching agent:

$$K = 2\left(\frac{D_e}{\pi}\right)^{0.5} \cdot \left(\frac{S}{V}\right) \quad (3)$$

As a result, the effective diffusion coefficient was calculated as follows:

$$D_e = \frac{K^2 \cdot \pi}{4} \cdot \left(\frac{V}{S}\right)^2 \quad (4)$$

Evaluation of the dominant leaching mechanism based on the dependence of the decimal logarithm of the accumulated fraction of leached radionuclide (B_t, mg/m^2) on the decimal logarithm of the leaching time t, s:

$$lg\,(B_t) = \frac{1}{2}\lg t + lg\left[U_{max} d\sqrt{\frac{D_e}{\pi}}\right] \quad (5)$$

where U_{max} is the maximum amount of leached radionuclide, mg/kg, d is the matrices density, kg/m^3.

The leaching depth of the matrices characterizes the destruction when the matrices as a whole is in an aqueous medium. This characteristic was calculated by Eq. (5):

$$L_t^i = \sum_1^n \left(W_n^i \cdot \frac{t_n}{d}\right) \quad (6)$$

L_t^i – matrices leaching depth achieved over a time interval t_n, cm, d – sample density, g/cm^3.

3. Results and discussion

3.1. XRD and FT-IR

The biogenic potassium aluminosilicate synthesized on the basis of rice straw was amorphous, a halo with a maximum of 2 θ about 29 deg. was observed on the diffractogram (Fig. 2a). After saturation with cesium ions, there were no noticeable changes in the XRD patterns. Fig. 2b shows the IR spectrum of the initial RS-$KAlSi_3O_8$ powder and the cesium form RS-(K,Cs)$AlSi_3O_8$. In the IR spectra of the samples (Fig. 2b), an intense absorption band in the region of 850–1100 cm^{-1} was recorded, associated with valence vibrations of Si–O–Si and Al–O–Al bonds. It should be noted that in a sample saturated with cesium, in comparison with the initial one, a slight shift of this absorption band to the region of lower frequencies was observed, which is associated with the softening of the structure of the nanocrystalline powder. Low-frequency absorption bands in the 450–600 cm^{-1} region were characteristic of deformation vibrations of Si–O–Si and Al–O–Si bonds.

The absorption bands in the 1600 and 3100–3650 cm^{-1} regions

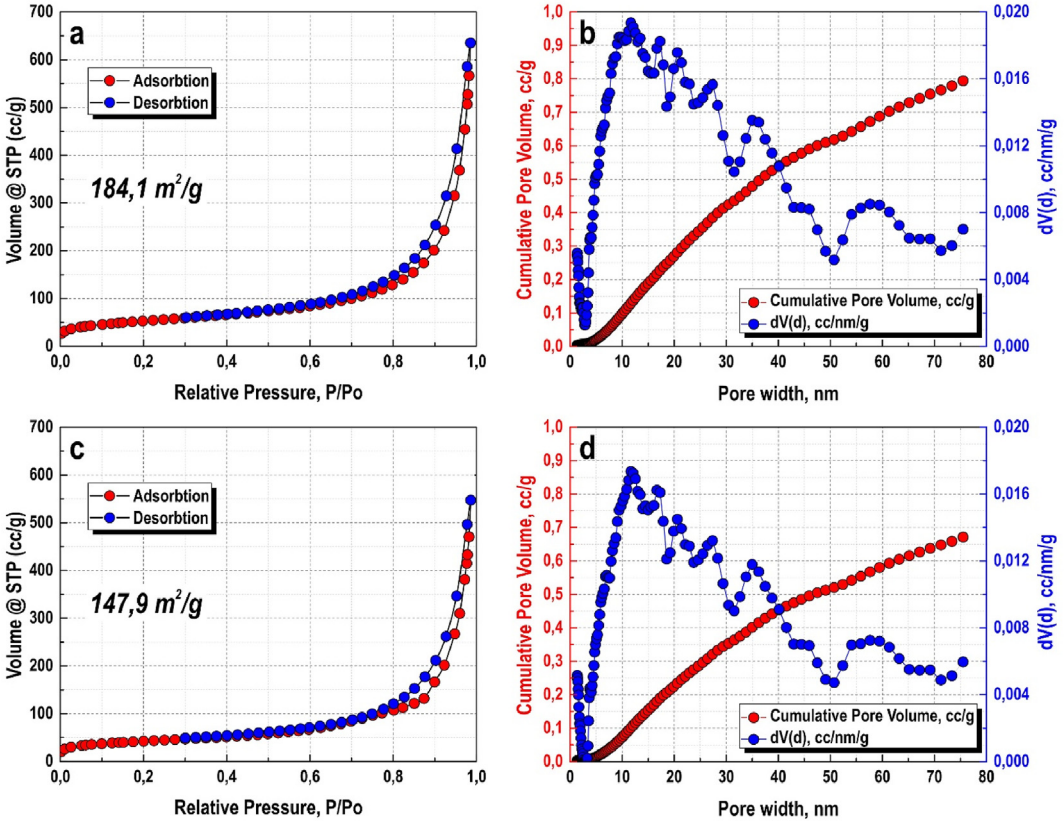

Fig. 5. Isotherms of low temperature nitrogen adsorption-desorption and DFT pore size distributions of *(a, b)* RS-$KAlSi_3O_8$ and *(c, d)* RS-(K,Cs)$AlSi_3O_8$ powder.

were caused by deformation and valence vibrations of crystallization water, respectively. The maximum absorption band of the water valence vibrations was 3450 cm^{-1} slightly lower for the valence vibrations of free water (~3600 cm^{-1}), and this was due to the presence of hydrogen bonds of water with the alumosilicate crystal lattice and a cation (potassium) compensating for the negative charge of the AlO_4 tetrahedron [40].

3.2. Cesium ions adsorption on RS-$KAlSi_3O_8$ aluminosilicate

Sorption properties to cesium ions were studied under static conditions from CsCl solutions with a concentration of 0.22–3.75 mmol/L. It was shown that the removal efficiency of cesium ions from the solution reached 96.6%. The sorption isotherm of cesium ions on the obtained material (Fig. 3) was well described by the Dubinin-Astakhov model (R^2 = 0.9995) and allowed to calculate the theoretical value of the maximum sorption capacity equal to 3.19 mmol/g.

Treatment of biogenic potassium aluminosilicate with an aqueous CsCl solution led to the substitution of potassium for cesium by the ion exchange mechanism, as was shown in Ref. [40]. At the same time, most of the potassium was replaced with cesium, and the real sorption capacity of biogenic aluminosilicate was 2.50 mmol/g, which is consistent with the theoretical value of the maximum sorption capacity calculated above.

3.3. Preparation of glass-ceramic composites

The granulometric composition of RS-(K,Cs)$AlSi_3O_8$ powder obtained from RS-$KAlSi_3O_8$ by saturation with cesium ions was represented by a wide fraction of particles with a size of 0.1–200 μm (Fig. 4). The smallest fraction was <1 μm, the average fraction was 1–20 μm in the form of agglomerates of smaller particles and a large fraction was represented by particles with a size of 20–200 μm. It was shown that fractions A and B make the main contribution to the particle size distribution and account for more than 80% of all particles, which was also confirmed by the SEM data (Fig. 4b). Some large particles were agglomerates of smaller fractions of particles with a size of 5–50 μm of spherical shape (Fig. 4b, area C) and less than 1 μm (Fig. 4b).

Nitrogen adsorption-desorption isotherms for samples belonged to type IV according to the IUPAC classification, characteristic of mesoporous bodies (Fig. 5a,c). The shape of the capillary-condensation hysteresis loop belonged to the H1 type, characteristic of open cylindrical pores, and had no saturation limit in the region of high p/p_0 ~0.95–0.99. Micro-, meso- and macropores in the studied samples were identified by DFT isotherms processing (Fig. 5b, d). This difference was due to the fact that sorption proceeds uniformly over the entire surface, so the distribution of pores did not change, but their volume decreased somewhat. The initial powder of potassium aluminosilicate RS-$KAlSi_3O_8$ had a high S_{BET} of 184.1 m^2/g. The sample of cesium aluminosilicate RS-(K,Cs)$AlSi_3O_8$ had a lower S_{BET} of 147.9 m^2/g.

According to dilatometric curves, it was determined that compaction (shrinkage) under conditions of spark plasma heating occurred in two stages (Fig. 6 a, b). Stage I was observed at the beginning of the process during the first minutes of synthesis (up to 2 min) at a temperature of 600–700 °C and mainly involved mechanical action on the powder by pressing. At this stage, the powder particles were deformed, crushed, regrouped and packed. The shrinkage rate for each sintering temperature (800–1000 °C) lied in the range of 2–3.2 mm/min. The main stage II, included the

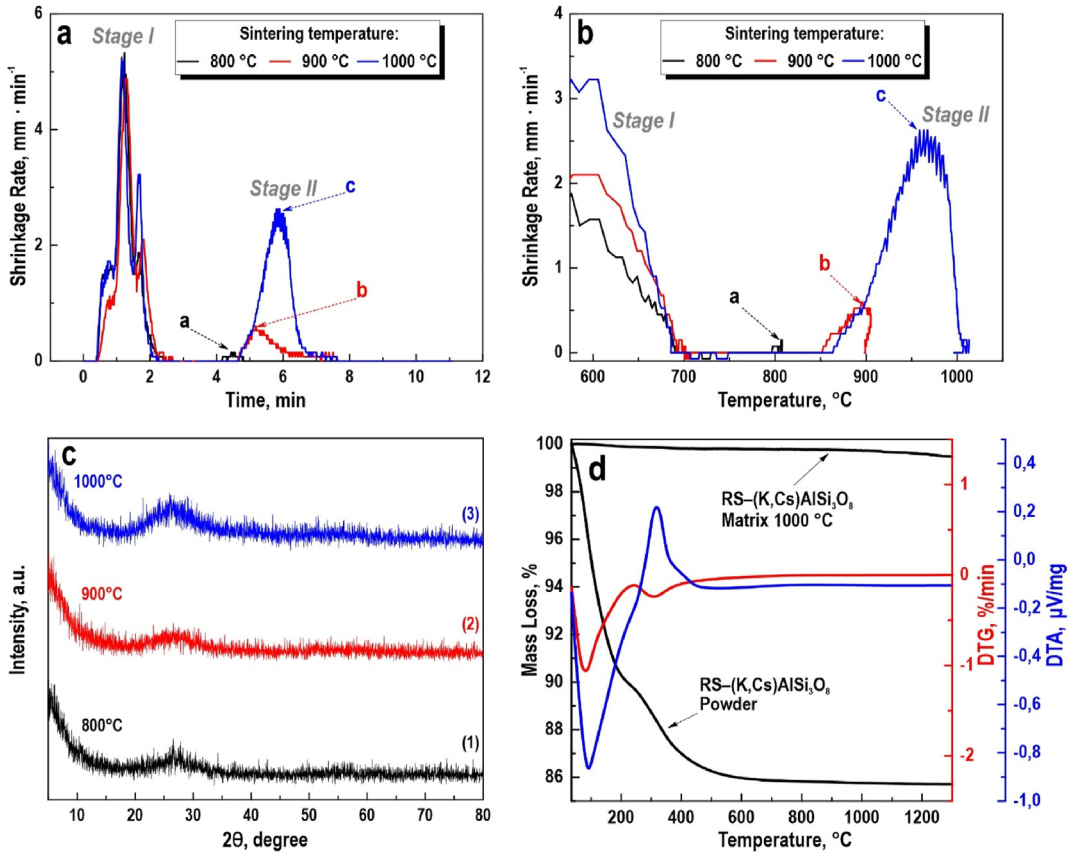

Fig. 6. (a), (b) dilatometry sintering curves of RS-(K,Cs)$AlSi_3O_8$, (c) XRD patterns of RS-(K,Cs)$AlSi_3O_8$ samples obtained by SPS at 800, 900, 1000°C and (d) DTA-TG analysis of RS-(K,Cs)$AlSi_3O_8$ powder and matrices calcined at 1000 °C.

thermal effect on the powder. It can be seen that the sintering of RS-(K,Cs)$AlSi_3O_8$ occurred only at temperatures of 900 and 1000 °C, the shrinkage rate was for 900 °C (curve b) – 1 mm/min, for 1000 °C (curve c) - 3 mm/min. Sintering of the material was accompanied by diffusion, plastic deformation and viscous flow of the material at grain boundaries. The above-mentioned processes lasted for 2 min at the subsequent exit to the plateau (Fig. 6a) According to the XRD data (Fig. 6c), amorphous cesium aluminosilicate did not crystallize during sintering at temperatures of 800–1000 °C and characteristic peaks were not observed.

It can be seen that for cesium-saturated sample (Fig. 6d) when the temperature rised, monotonous removal of water occurs without separation at the stage of water desorption, decomposition of crystallohydrates. The removal of the bulk of the water occurred at 600 °C and ended at about 1000 °C with a total weight loss of 24%. DTA for ceramics obtained at 1000 °C, weight loss was not observed up to 900 °C, only at higher temperatures there was a small decrease in mass <1 wt%, which is associated with the removal of carbon residues from rice straw.

The structure of consolidated ceramic samples varied depending on the process temperature (Fig. 7). The SEM image of the sample surface prepared at 800 °C showed that at this temperature sintering processes were only initiated, both sintered areas and areas where consolidation processes had just begun were present in the volume (Fig. 4a). Elongated sintered regions were formed in the structure of the sample during sintering, from which the formation of a glass phase in the sample was initiated.

Thus, the hardness and compressive strength were not high values of 0.235 GPa and 20.7 MPa, respectively (Table 1). According to the EDX analysis (Fig. 7a), these regions had a homogeneous composition, without recrystallization. The surface of the material had a porous heterogeneous structure. When the temperature raised to 900 °C, the area of agglomerates increased due to a more active temperature effect on RS-(K,Cs)$AlSi_3O_8$ intensification of solid-phase sintering of the material. The number of large pores and small particles in the sample sharply decreased (Fig. 7 b,c). In the inserts to Fig. 7a * -b * it can be seen that sintered agglomerates had areas with a porous internal volume. The type, size and structure of the pores decreased with increasing SPS temperature. This was due to two factors: firstly, the intensification of sintering processes, which were accompanied by diffusion and led to deformation and pores destruction (Fig. 5b).

When the temperature reached 1000 °C RS-(K,Cs) $AlSi_3O_8$ was characterized by an amorphous structure due to the partial formation of the glass phase. Under such conditions, a monolithic material with a maximum density of 2624 g/cm^3 and a high compressive strength of 231.3 MPa was obtained (Table 2).

It was found that the physical and mechanical characteristics of RS-(K,Cs)$AlSi_3O_8$ glass-ceramic matrices change with increasing SPS temperature in the range of 800–1000 °C. The density of the matrices varies up to 2.5086–2.6236 g/cm3. The compressive strength was in the range of 20.7–231.3 MPa, and the Vickers microhardness was 0.235–2.197 GPa (Table 1). Both of these values increased sharply at a sintering temperature above 900 °C. This

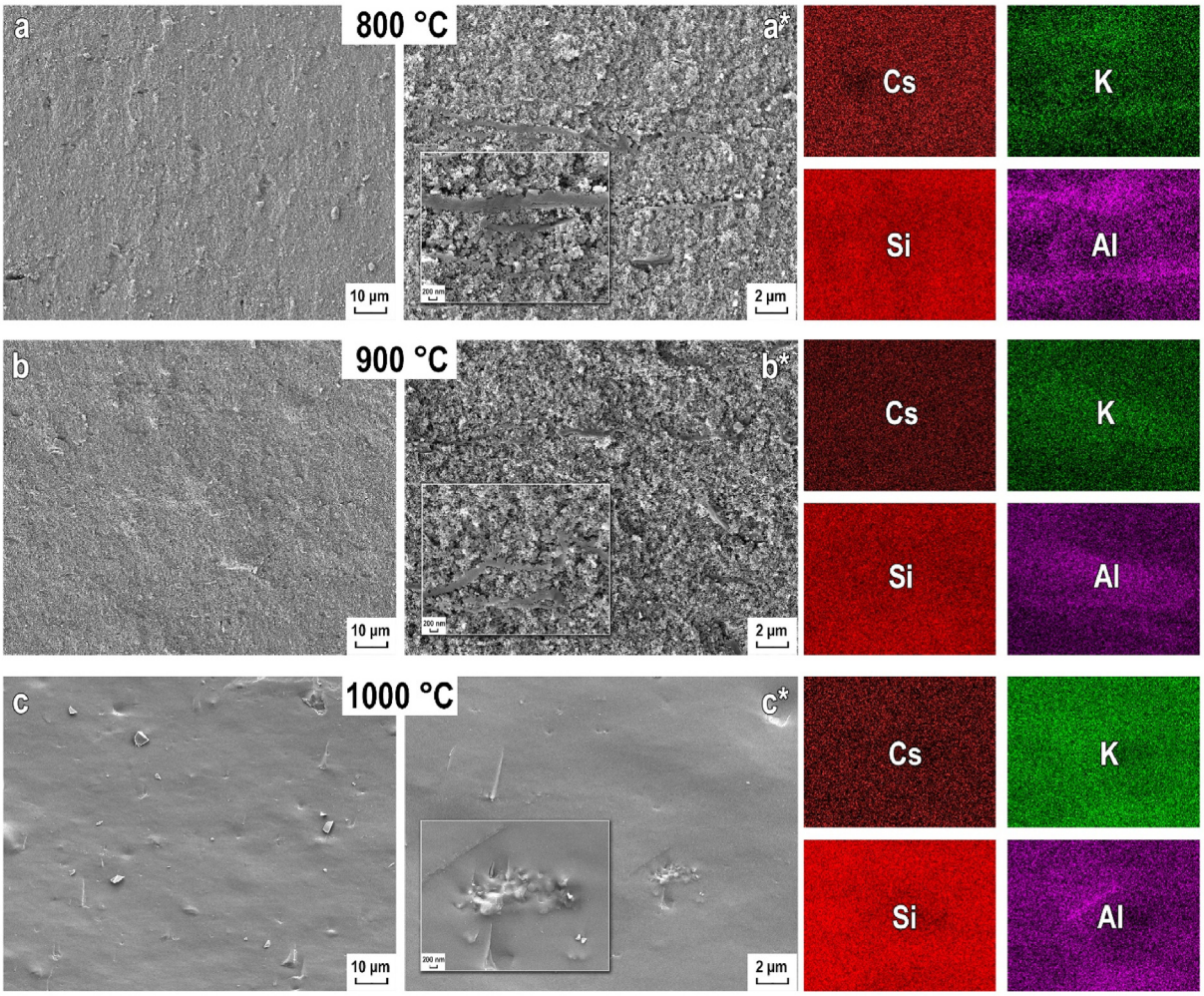

Fig. 7. SEM images and EDX analysis of RS-(K,Cs)$AlSi_3O_8$ ceramics samples obtained by SPS at 800, 900 and 1000 °C.

Table 1
Characteristics of the matrixes containing cesium obtained.

Sintering temperature, °C	Density, g/cm^3	Comprehensive strength, MPa	Hardness, GPa	Leaching rate (R_{Cs}), g·cm^{-2}·day^{-1}
800	2.509	20.7	0.235	$1.05 \times 10^{-4} - 2.2 \times 10^{-6}$
900	2.559	127.4	1.481	$8.23 \times 10^{-5} - 1.95 \times 10^{-6}$
1000	2.624	231.3	2.197	$2.18 \times 10^{-6} - 1.37 \times 10^{-7}$

Table 2
Quality characteristics for solid-state matrices.

Parameter	Value		
	According to GOST R 50926-96	Matrices prepared by SPS at 1000°C	Control method
Leaching rate of ^{133}Cs, g/cm^2·day	$<10^{-5}$	$1.37 \cdot 10^{-7}$	GOST R 52126-2003 (ISO 6961:1982)
Comprehensive strength, MPa	>9	231.3	Tests on a bursting machine
Thermal stability, °C	>550	Up to 1000	XRD, DTA-TG
Uniformity of the structure in the volume of the glass block	Homogeneous	Homogeneous	XRD and SEM

effect was probably associated with a change in the sintering rate of the matrices (Fig. 6b), at a temperature above 900 °C, intensive sintering and collapse of the open porosity and the formation of a monolithic glass-ceramic structure occurred. An increase in the dispersion and asymmetry of the distribution of microhardness values relative to the statistical median line in the box-and-whiskers diagram indicated an increase in the structural heterogeneity of the single-phase synthetic RS-(K,Cs)$AlSi_3O_8$ with an increase in the SPS temperature (Fig. 8). The range of microhardness values in the statistical sample was due to the anisotropy of the

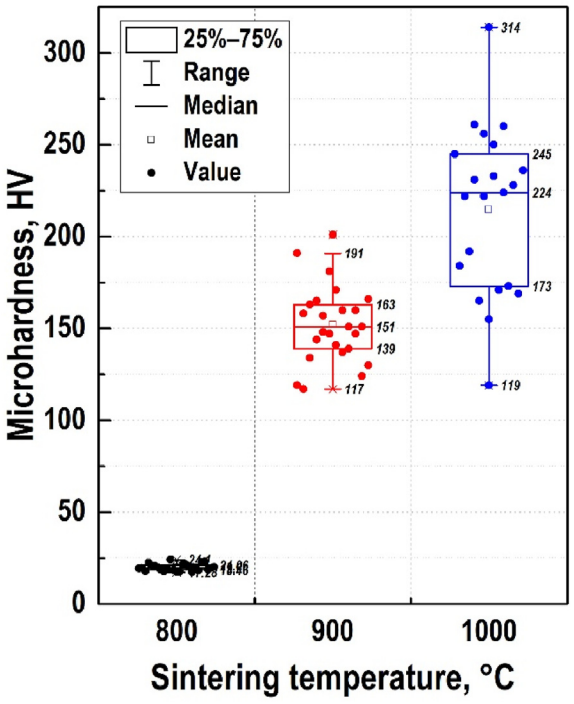

Fig. 8. Vickers microhardness values for samples RS-(K,Cs)$AlSi_3O_8$ prepared by SPS at 800, 900, 1000°C

Table 3
Effective cesium diffusion coefficient of the RS-(K,Cs)$AlSi_3O_8$ glass-ceramic samples obtained by SPS at 800, 900, 1000°C

Time, days	Effective cesium diffusion coefficient, cm^2/s		
	800°C	900°C	1000°C
1	2.93×10^{-10}	6.27×10^{-9}	8.16×10^{-12}
3			
7			9.07×10^{-14}
14	2.41×10^{-10}		
21	2.70×10^{-11}	8.97×10^{-10}	
30			

of the released cesium fraction on the logarithm of time (Fig. 9b) was characterized by the tangent angle tangent close to 1, which, according to the de Groot and van der Sloot model [40,41], indicates the effect of surface leaching: cesium fixed in the surface layers of samples leaches faster than the diffusion of cesium from the volume of ceramics to the surface. After the break point in all tested samples, diffusion within the material become the limiting stage of cesium leaching. Thus, glass ceramics were characterized by a low cesium diffusion coefficient (Fig. 9c), which was associated with a low number of structural defects in the material and the collapse of pores during sintering.

Table 3 shows the calculated diffusion coefficients of strontium from ceramic samples depending on the leaching time. As the duration of the experiment increased, the diffusion coefficient decreased, which was associated with a decrease in the strontium

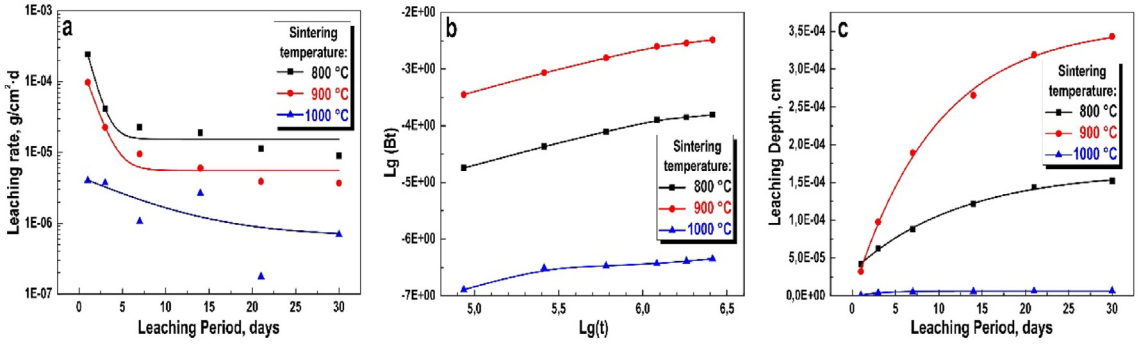

Fig. 9. Parameters of cesium leaching from RS-(K,Cs)$AlSi_3O_8$ matrices prepared by SPS at 800, 900, 1000 °C: (a) rate of cesium leaching; (b) logarithmic dependences of the accumulated fraction of leached cesium on the leaching time; (c) – leaching depth.

properties formed as a result of partial crystallization of the obtained glass ceramics.

The cesium leaching from obtained RS-(K,Cs)$AlSi_3O_8$ ceramic samples was evaluated, which is the main indicator of their effectiveness for the immobilization of cesium radionuclides. The rate of cesium leaching was the lowest for samples obtained at 1000 °C (Fig. 9a). This indicator reached 10^{-6}-10^{-7} g/cm^2 day, which met the requirements of GOST R 50926 96 for solid high-level waste. Obviously, the high hydrolytic stability of the samples of aluminosilicate matrices was due to their glass-like composition based on RS-(K,Cs)$AlSi_3O_8$ without any recrystallization during sintering.

The leaching curves of cesium ions were characterized by break points: day 14 for samples with a sintering temperature of 800 and 900 °C, day 3 for a sample with a sintering temperature of 1000 °C (Fig. 9a). Up to the breaking point, the dependence of the logarithm content in the near-surface layers of the samples and, thus, a change in the mechanism of removal of the substance.

4. Conclusions

Amorphous alumosilicate RS-$KAlSi_3O_8$ with a high sorption capacity to cesium ions of 3.2 mmol/g was synthesized by processing rice straw by precipitation from alkaline hydrolysate. Solid-state amorphous matrices for ^{137}Cs immobilization of amorphous composition based on the synthesized RS-(K,Cs)$AlSi_3O_8$ powder were obtained by the SPS method. The thermal stability of the initial aluminosilicate and the cesium-saturated RS-(K,Cs)$AlSi_3O_8$ form during heat treatment in an inert medium up to 1000 °C was shown. The obtained matrices with a uniform distribution of cesium by volume had high values of density (2.62 g/cm^3),

compressive strength (231.3 MPa) and Vickers microhardness (2.197 GPa). The highest resistance to dissolution was possessed by high-temperature samples obtained at 1000 °C, where the rate of cesium leaching (R_{Cs}) did not exceed 1.37×10^{-7} g $cm^{-2} \times day^{-1}$, and the diffusion coefficient (D_e) was 9.07×10^{-14} cm^2/s. The high quality of the obtained matrices was confirmed by compliance with GOST R 50926-96. The developed aluminosilicate matrices based on agricultural waste are prospect for purification technologies and processing of radioactive waste, the creation of radioisotope products.

Declaration of competing interest

The authors declare that they have no known competing financial interests or personal relationships that could have appeared to influence the work reported in this paper.

Acknowledgement

Synthesis of initial powders, saturation with cesium ions, AAS and XRD analyses were carried out in the Institute of Chemistry FEB RAS within the State Assignment of the Ministry of Science and Higher Education of the Russian Federation Themes № 0205-2021-0001, 0205-2021-0002.

Synthesis and characterization of ceramics samples were financially supported by State Assignment of the Ministry of Science and Higher Education of the Russian Federation topic number 00657-2020-0006. The study of calculation of cesium leaching and density studies were studied by the financial support of the Russian Foundation for Basic Research, project No. 19-33-90150. The investigation was financially supported by Russian Science Foundation (project No. 21-73-00304).

The work involved equipment of integrated common use center and interdisciplinary in the field of nanotechnologies and new functional materials (Far Eastern Federal University, Vladivostok, Russia), and also common use center “Far Eastern Center for Structural Research” (Institute of Chemistry, Far Eastern Branch of the Russian Academy of Sciences, Vladivostok, Russia).

References

[1] P. Szajerski, A. Bogobowicz, A. Gasiorowski, Cesium retention and release from sulfur polymer concrete matrix under normal and accidental conditions, J. Hazard Mater. 381 (2020) 121180, https://doi.org/10.1016/j.jhazmat.2019.121180.

[2] M.Z. Jacobson, Review of solutions to global warming, air pollution, and energy security, Energy Environ. Sci. 2 (2009) 148–173, https://doi.org/10.1039/b809990c.

[3] S.J. Zinkle, G.S. Was, Materials challenges in nuclear energy, Acta Mater. 61 (2013) 735–758, https://doi.org/10.1016/j.actamat.2012.11.004.

[4] M. Chino, H. Nakayama, H. Nagai, H. Terada, G. Katata, H. Yamazawa, Preliminary estimation of release amounts of 131i and 137cs accidently discharged from the fukushima daiichi nuclear power plant into the atmosphere, J. Nucl. Sci. Technol. 48 (2011) 1129–1134, https://doi.org/10.1080/18811248.2011.9711799.

[5] L.H. Ortega, M.D. Kaminski, S.M. McDeavitt, Pollucite and feldspar formation in sintered bentonite for nuclear waste immobilization, Appl. Clay Sci. 50 (2010) 594–599, https://doi.org/10.1016/j.clay.2010.10.003.

[6] O.O. Shichalin, E.K. Papynov, V.Y. Maiorov, A.A. Belov, E.B. Modin, I.Y. Buravlev, Y.A. Azarova, A.V. Golub, E.A. Gridasova, A.E. Sukhorada, I.G. Tananaev, V.A. Avramenko, Spark plasma sintering of aluminosilicate ceramic matrices for immobilization of cesium radionuclides, Radiochemistry 61 (2019) 185–191, https://doi.org/10.1134/S1066362219020097.

[7] S.B. Yarusova, O.O. Shichalin, A.A. Belov, S.A. Azon, I.Y. Buravlev, A.V. Golub, V.Y. Mayorov, A.V. Gerasimenko, E.K. Papynov, A.I. Ivanets, A.A. Buravleva, B. Merkulov, V.A. Nepomnyushchaya, O.V. Kapustina, P.S. Gordienko, Synthesis of amorphous KAlSi 3 O 8 for cesium radionuclide immobilization into solid matrices using spark plasma sintering technique, Ceram. Int. (2021), https://doi.org/10.1016/j.ceramint.2021.10.164.

[8] O.O. Shichalin, E.K. Papynov, V.A. Nepomnyushchaya, A.I. Ivanets, A.A. Belov, A.N. Dran'kov, S.B. Yarusova, I.Y. Buravlev, A.E. Tarabanova, A.N. Fedorets, S.A. Azon, Z.E. Kornakova, S.Y. Budnitskiy, I.G. Tananaev, Y. Shi, Y. Xiong, H. Wang, Hydrothermal synthesis and spark plasma sintering of NaY zeolite as solid-state matrices for cesium-137 immobilization, J. Eur. Ceram. Soc. (2022), https://doi.org/10.1016/j.jeurceramsoc.2022.02.007.

[9] I. Yanase, S. Tamai, H. Kobayashi, Sintering of pollucite using amorphous powder and its low thermal expansion property, J. Ceram. Soc. Japan. 111 (2003) 533–536, https://doi.org/10.2109/jcersj.111.533.

[10] S.K. Jesudoss, J.J. Vijaya, K. Kaviyarasu, L.J. Kennedy, R. Jothi Ramalingam, H.A. Al-Lohedan, Anti-cancer activity of hierarchical ZSM-5 zeolites synthesized from rice-based waste materials, RSC Adv. 8 (2018) 481–490, https://doi.org/10.1039/C7RA11763A.

[11] A.I. Orlova, M.I. Ojovan, Ceramic mineral waste-forms for nuclear waste immobilization, Materials (Basel) 12 (2019), https://doi.org/10.3390/ma12162638.

[12] E.K. Papynov, O.O. Shichalin, M.A. Medkov, D.N. Grishchenko, I.A. Tkachenko, A.N. Fedorets, V.S. Pechnikov, A.V. Golub, I.Y. Buravlev, I.G. Tananaev, V.A. Avramenko, Spark plasma sintering of special-purpose functional ceramics based on UO2, ZrO2, Fe3O4/α-Fe2O3, Glas, Phys. Chem. 44 (2018) 632–640, https://doi.org/10.1134/S1087659618060159.

[13] E.K. Papynov, O.O. Shichalin, A.Y. Mironenko, A.V. Ryakov, I.V. Manakov, P.V. Makhrov, I.Y. Buravlev, I.G. Tananaev, V.A. Avramenko, V.I. Sergienko, Synthesis of high-density pellets of uranium dioxide by spark plasma sintering in dies of different types, Radiochemistry 60 (2018) 362–370, https://doi.org/10.1134/S1066362218040045.

[14] E.K. Papynov, A.S. Portnyagin, E.B. Modin, V.Y. Mayorov, O.O. Shichalin, A.P. Golikov, V.S. Pechnikov, E.A. Gridasova, I.G. Tananaev, V.A. Avramenko, A complex approach to assessing porous structure of structured ceramics obtained by SPS technique, Mater. Char. 145 (2018) 294–302, https://doi.org/10.1016/j.matchar.2018.08.044.

[15] I.O. Ali, T.M. Salama, M.S. Thabet, K.S. El-Nasser, A.M. Hassan, Encapsulation of ferro- and ferricyanide complexes inside ZSM-5 zeolite synthesized from rice straw: implications for synthesis of Prussian blue pigment, Mater. Chem. Phys. 140 (2013) 81–88, https://doi.org/10.1016/j.matchemphys.2013.02.069.

[16] R.J. Lawson, M.B. Schenker, S.A. McCurdy, B. Jenkins, L.A. Lischak, W. John, D. Scales, Exposure to amorphous silica fibers and other particulate matter during pace farming operations, Appl. Occup. Environ. Hyg 10 (1995) 677–684, https://doi.org/10.1080/1047322X.1995.10387666.

[17] I. Health, A. Iron, O. Medicine, By Rice, 1995.

[18] C.R. Melo, A.C. Francisco, N.C. Kuhnen, M.R. da Rocha, A.R. Melo, H.G. Riella, E. Angioletto, Production of zeolite from rice husk ash, Mater. Sci. Forum 798–799 (2014) 617–621. https://doi.org/10.4028/www.scientific.net/MSF.798-799.617.

[19] R.M. Mohamed, I.A. Mkhalid, M.A. Barakat, Rice husk ash as a renewable source for the production of zeolite NaY and its characterization, Arab. J. Chem. 8 (2015) 48–53, https://doi.org/10.1016/j.arabjc.2012.12.013.

[20] E.-P. Ng, G.K. Lim, G.-L. Khoo, K.-H. Tan, B.S. Ooi, F. Adam, T.C. Ling, K.-L. Wong, Synthesis of colloidal stable Linde Type J (LTJ) zeolite nanocrystals from rice husk silica and their catalytic performance in Knoevenagel reaction, Mater. Chem. Phys. 155 (2015) 30–35, https://doi.org/10.1016/j.matchemphys.2015.01.061.

[21] V. Charitha, V.S. Athira, V. Jittin, A. Bahurudeen, P. Nanthagopalan, Use of different agro-waste ashes in concrete for effective upcycling of locally available resources, Construct. Build. Mater. 285 (2021), 122851, https://doi.org/10.1016/j.conbuildmat.2021.122851.

[22] H.R. Khalid, N.K. Lee, S.M. Park, N. Abbas, H.K. Lee, Synthesis of geopolymer-supported zeolites via robust one-step method and their adsorption potential, J. Hazard Mater. 353 (2018) 522–533, https://doi.org/10.1016/j.jhazmat.2018.04.049.

[23] Y. Liu, C. Yan, Z. Zhang, H. Wang, S. Zhou, W. Zhou, A comparative study on fly ash, geopolymer and faujasite block for Pb removal from aqueous solution, Fuel 185 (2016) 181–189, https://doi.org/10.1016/j.fuel.2016.07.116.

[24] Q. Ge, M. Moeen, Q. Tian, J. Xu, K. Feng, Highly effective removal of Pb2+ in aqueous solution by Na-X zeolite derived from coal gangue, Environ. Sci. Pollut. Res. 27 (2020) 7398–7408, https://doi.org/10.1007/s11356-019-07412-z.

[25] C.B. Durrant, J.D. Begg, A.B. Kersting, M. Zavarin, Cesium sorption reversibility and kinetics on illite, montmorillonite, and kaolinite, Sci. Total Environ. 610–611 (2018) 511–520, https://doi.org/10.1016/j.scitotenv.2017.08.122.

[26] E.K. Papynov, O.O. Shichalin, V.Y. Mayorov, V.G. Kuryavyi, T.A. Kaidalova, L.V. Teplukhina, A.S. Portnyagin, A.B. Slobodyuk, A.A. Belov, I.G. Tananaev, V.A. Avramenko, V.I. Sergienko, SPS technique for ionizing radiation source fabrication based on dense cesium-containing core, J. Hazard Mater. 369 (2019) 25–30, https://doi.org/10.1016/j.jhazmat.2019.02.016.

[27] N.K. Lee, H.R. Khalid, H.K. Lee, Adsorption characteristics of cesium onto mesoporous geopolymers containing nano-crystalline zeolites, Microporous Mesoporous Mater. 242 (2017) 238–244, https://doi.org/10.1016/j.micromeso.2017.01.030.

[28] F.E. Titchou, R.A. Akbour, A. Assabbane, M. Hamdani, Removal of cationic dye from aqueous solution using Moroccan pozzolana as adsorbent: isotherms, kinetic studies, and application on real textile wastewater treatment, Groundw. Sustain. Dev. 11 (2020), 100405, https://doi.org/10.1016/j.gsd.2020.100405.

[29] S. Wang, Y. Boyjoo, A. Choueib, Z.H. Zhu, Removal of dyes from aqueous solution using fly ash and red mud, Water Res. 39 (2005) 129–138, https://doi.org/10.1016/j.watres.2004.09.011.

[30] H. Nsubuga, C. Basheer, M.B. Haider, R. Bakdash, Sol-gel based biogenic silica

composite as green nanosorbent for chemometric optimization of micro-solid-phase extraction of beta blockers, J. Chromatogr. A 1554 (2018) 16–27, https://doi.org/10.1016/j.chroma.2018.04.044.
[31] O.V. Buyko, S.I. Metelitsa, V.N. Losev, A.E. Panasenko, A.F. Shimanskii, Biosilica layer-by-layer modified with polyamines and carboxyarsenazo for REE pre-concentration prior to ICP-MS determination in lignites and volcanic fumarole sediment, Anal. Methods 12 (2020) 3813–3822, https://doi.org/10.1039/D0AY00624F.
[32] P. Sazama, O. Bortnovsky, J. Dědeček, Z. Tvarůžková, Z. Sobalík, Geopolymer based catalysts—new group of catalytic materials, Catal. Today 164 (2011) 92–99, https://doi.org/10.1016/j.cattod.2010.09.008.
[33] N.P. Shapkin, I.G. Khal'chenko, A.A. Yudakov, V.I. Sergienko, A.E. Panasenko, V.Y. Maiorov, L.B. Leont'ev, Synthesis of a nanocomposite based on polyethylene and modified vermiculite, Inorg. Mater. 53 (2017) 1091–1096, https://doi.org/10.1134/S0020168517100120.
[34] R.A. Bakar, R. Yahya, S.N. Gan, Production of high purity amorphous silica from rice husk, Procedia Chem. 19 (2016) 189–195, https://doi.org/10.1016/j.proche.2016.03.092.
[35] A.M.N. Moudio, H.K. Tchakouté, D.L.V. Ngnintedem, F. Andreola, E. Kamseu, C.P. Nanseu-Njiki, C. Leonelli, C.H. Rüscher, Influence of the synthetic calcium aluminate hydrate and the mixture of calcium aluminate and silicate hydrates on the compressive strengths and the microstructure of metakaolin-based geopolymer cements, Mater. Chem. Phys. 264 (2021), https://doi.org/10.1016/j.matchemphys.2021.124459.
[36] W. Simanjuntak, K.D. Pandiangan, Z. Sembiring, A. Simanjuntak, S. Hadi, The effect of crystallization time on structure, microstructure, and catalytic activity of zeolite-A synthesized from rice husk silica and food-grade aluminum foil, Biomass Bioenergy 148 (2021), 106050, https://doi.org/10.1016/j.biombioe.2021.106050.
[37] E.A. Abdelrahman, Y.G. Abou El-Reash, H.M. Youssef, Y.H. Kotp, R.M. Hegazey, Utilization of rice husk and waste aluminum cans for the synthesis of some nanosized zeolite, zeolite/zeolite, and geopolymer/zeolite products for the efficient removal of Co(II), Cu(II), and Zn(II) ions from aqueous media, J. Hazard Mater. 401 (2021) 123813, https://doi.org/10.1016/j.jhazmat.2020.123813.
[38] Properties of fly ash and rice husk ash blended geopolymer with sodium aluminate as activator solution | Eng. Appl. Sci. Res., (n.d.).
[39] S.B. Yarusova, P.S. Gordienko, A.E. Panasenko, N.N. Barinov, L.A. Zemnukhova, Sorption properties of sodium and potassium aluminosilicates from alkaline hydrolyzates of rice straw, Russ. J. Phys. Chem. A 93 (2019) 333–337, https://doi.org/10.1134/S003602441902033X.
[40] D.S. Kosson, H.A. van der Sloot, T.T. Eighmy, An approach for estimation of contaminant release during utilization and disposal of municipal waste combustion residues, J. Hazard Mater. 47 (1996) 43–75, https://doi.org/10.1016/0304-3894(95)00109-3.
[41] G. de Groot, H. van der Sloot, Determination of leaching characteristics of waste materials leading to environmental product certification, in: Stab. Solidif. Hazardous, Radioact. Mix. Wastes 2nd Vol., ASTM International, 100 Barr Harbor Drive, PO Box C700, West Conshohocken, PA 19428-2959, n.d.: pp. 149–149–22. doi:10.1520/STP19548S.